


Article

Optimization Parameters, Kinetics, and Mechanism of Naproxen Removal by Catalytic Wet Peroxide Oxidation with a Hybrid Iron-Based Magnetic Catalyst

Ysabel Huacalco-Aguilar ^{1,2}, Silvia Álvarez-Torrellas ¹, Marcos Larriba ¹, V. Ismael Águeda ¹, José Antonio Delgado ¹ , Gabriel Ovejero ¹ and Juan García ^{1,*}

¹ Catalysis and Separation Processes Group, Chemical Engineering and Materials Department, Faculty of Chemistry, Complutense University, Avda. Complutense s/n, 28040 Madrid, Spain; Ysabelhu@ucm.es (Y.H.-A.); satorrellas@ucm.es (S.Á.-T.); marcoslarriba@ucm.es (M.L.); viam@ucm.es (V.I.Á.); jadelob@ucm.es (J.A.D.); govejero@ucm.es (G.O.)

² Departamento de Ingeniería Química, Universidad Nacional de San Agustín, Av. Independencia s/n, 04001 Arequipa, Peru

* Correspondence: jgarciar@ucm.es; Tel.: +34-913-945-207

Received: 13 February 2019; Accepted: 15 March 2019; Published: 20 March 2019



Abstract: This work presents a study of the assessment of the operating parameters of the catalytic wet peroxide oxidation (CWPO) of naproxen (NAP) using magnetite/multi-walled carbon nanotubes (Fe₃O₄/MWCNTs) as a catalyst. The effect of pH, temperature, and H₂O₂ dosage on CWPO process was evaluated by using the response surface model (RSM), allowing us to obtain an optimum NAP removal of 82% at the following operating conditions: pH = 5, T = 70 °C, [H₂O₂]₀ = 1.5 mM, and [NAP]₀ = 10.0 mg/L. Therefore, NAP degradation kinetics were revealed to follow a pseudo-second-order kinetic model, and an activation energy value of 4.75 kJ/mol was determined. Adsorption and using only H₂O₂ experiments, both considered as blank tests, showed no significant removal of the pollutant. Moreover, Fe₃O₄/MWCNTs material exhibited good recyclability along three consecutive cycles, finding an average NAP removal percentage close to 80% in each cycle of 3 h reaction time. In addition, the scavenging tests confirmed that the degradation of NAP was mainly governed by •OH radicals attack. Two reaction sequences were proposed for the degradation mechanism according to the detected byproducts. Finally, the versatility of the catalyst was evidenced in the treatment of different environmentally relevant aqueous matrices (wastewater treatment plant effluent (WWTP), surface water (SW), and a hospital wastewater (HW)) spiked with NAP, obtaining total organic carbon (TOC) removal efficiencies after 8 h in the following order: NAP-SW > NAP-HW > NAP-WWTP.

Keywords: CWPO; magnetic catalyst; naproxen; response surface methodology; wastewater

1. Introduction

Pharmaceutical compounds are an important part of toxic materials in wastewater that are currently growing around the world [1]. They have been frequently detected in the aqueous medium, supposing a growing environmental problem for the scientific community. The excessive drug production demanded and consumed by humans and animals usually ends up in surface water [1], sewage effluents [2], groundwater [3], and even drinking water [4] due to the discharges from municipal wastewater treatment plants (WWTPs) [1], and, consequently, these contaminants can lead to devastating effects on the environment [3,5]. Particularly, non-steroidal anti-inflammatory drugs (NSAIDs) have been found in water effluents at increasing concentrations and their removal from the environment is becoming a real challenge [6]. In this work, naproxen (NAP) has been selected due

to its presence in many kinds of water environments [7–9], such as WWTPs effluents, surface water, and hospital wastewater effluent, in significant concentrations (<0.1 ng/L to 0.220 mg/L) [2,7–10]. Despite the low values found (from ng/L to mg/L), the risk assessment associated with the risk quotient (RQ) of NAP has been reported in 84 fish, which is considered as a very high value, and consequently, demands the development of efficient alternative treatments of aqueous matrices containing NAP [10]. Moreover, the toxicological studies demonstrated that NAP and their degradation byproducts exhibited adverse effects on aquatic organisms at an EC_{50} value of 0.33 mg/L on *C. dubia* [11]. In addition, the NAP molecule is highly stable at neutral and basic pH media and its dissociation only occurs when it is heated in concentrated acid sulfuric/nitric solutions [12,13]. These properties make it difficult to be degraded in the conventional WWTPs that usually work near the neutral pH. As a consequence, NAP would pass through these conventional treatment processes and end up in the water environment [14]. In this sense, the effectiveness of the removal of NAP from wastewater by different treatments, such as adsorption in activated process, biological degradation, photolysis, ozonation/ H_2O_2 , and adsorption on activated carbon, were 50–80%, no data, 99–100%, 98%, and 52%, respectively [2]. In 2013, Ma et al. [15] demonstrated that the generated derivate products by photo-degradation of NAP were more toxic than the parent compound. Accordingly, research on methods of NAP removal is becoming an interesting challenge, especially if the resulting derivate products are less toxic and more biodegradable than NAP [2].

Catalytic wet peroxide oxidation (CWPO) is an advanced oxidation process where the heterogeneous catalyst catalyzes the decomposition of hydrogen peroxide into oxygen-based radicals at mild conditions of temperature and pressure [16]. The reactive species ($\bullet OH$) are able to degrade even the most recalcitrant organic molecules and convert them into less persistent and non-contaminant compounds [16]. CWPO was demonstrated to be effective for the removal of refractory organic compounds, traceable organic contaminants, or some inorganic pollutants, or in particular cases, to increase the wastewater biodegradability as a pretreatment of a subsequent biological treatment stage [1,17–19]. Heterogeneous CWPO reactions using magnetite (Fe_3O_4) supported on multi-walled carbon nanotubes (MWCNTs) as a catalyst were reported for the effective removal of methylene blue [20], sulfamethazine [21], 17α -methyltestosterone [22], and atrazine [23]. Furthermore, Fe_3O_4 /MWCNTs material has been reported to show interesting properties such as the wide-range pH of work, stability, recyclability, and low toxicity towards the medium, making this catalyst an effective alternative for the treatment of different toxic compounds in wastewater. It is noteworthy to say that MWCNTs acting as catalytic support plays an important role for the dispersion of the magnetite into the surface, obtaining a minimum leaching of the phase active and allowing it to work at a wider pH range [20–25]. Indeed, the surface of the MWCNTs has been reported to be chemically functionalized to potentially enhance the density of the active sites responsible for the $\bullet OH$ generation, promoting the $\bullet OH$ species formation [25]. In addition, MWCNTs are also known to be relatively stable in extreme environments, maintaining their mechanical properties along the process [25]. Therefore, Fe_3O_4 /MWCNTs catalysts can be more effective in the degradation of pollutants compared to those immobilized on carriers, where the separation and recovering of the solids is needed after the treatment. In this context, Fe_3O_4 /MWCNTs material is an effective alternative for the easy separation of the solid from the aqueous solution by using a magnet [23,26]. The synthesis of the catalyst was assessed following the combination of two known methods (co-precipitation and hydrothermal method) [27]. To the best of the authors' knowledge, this is the first work based on the synthesis of a magnetic material (Fe_3O_4 /MWCNTs) used in CWPO reactions for effective NAP degradation. The catalyst was also tested in different aqueous matrices spiked with the pollutant.

This study has been structured in four stages. The first stage was to follow a facile synthesis route of the catalyst based on the incorporation of magnetite on the surface of MWCNTs, obtaining the magnetic solid further used in the CWPO experiments. The morphological structure of the material was studied by transmission electron microscopy (TEM). Moreover, the textural and surface-chemical properties of the catalyst were fully explored. Our second aim was to evaluate the effect of the operating

parameters (H_2O_2 dose, pH, and temperature) on the CWPO process for the removal of NAP by using a response surface methodology (RSM) based on the Box–Behnken Design (BBD), allowing us to determine the optimal experimental conditions. As a third aim, the kinetics of the catalytic degradation of the drug was explored, the activation energy was calculated, and a degradation mechanism of the pollutant was proposed. In addition, the reusability and recyclability of the catalyst were evaluated. Finally, our fourth aim was to test the optimum CWPO process in three real aqueous matrices—a wastewater treatment plant effluent (WWTP), surface water (SW), and a hospital wastewater (HW) spiked with NAP—determining the total organic carbon (TOC) removal, the efficiency of H_2O_2 , and the toxicity of the effluent after 8 h reaction time.

2. Results and Discussion

2.1. Catalyst Characterization

Firstly, in the TEM images it can be seen that the multi-walled carbon nanotubes (MWCNTs) showed a particle size lower than 50 nm (Figure 1a). Moreover, Fe_3O_4 particles with diameters ranging from 10 to 20 nm were in a sphere-like shape in the prepared catalyst (Fe_3O_4 -MWCNTs) (Figure 1b), revealing that the iron oxide magnetite nanoparticles were successfully decorated on the surface of the MWCNTs. No changes in the morphology on the catalyst was observed after the second reuse (Figure 1c), where the magnetic particles maintain their spherical shape. This fact confirmed the high reliability of the applied synthesis method.

The thermogravimetric analysis (TGA) of the untreated MWCNTs, functionalized MWCNTs, and fresh and reused catalyst are shown in Figure 1d. The catalyst and functionalized MWCNTs can be considered thermally stable up to 400 °C under air atmosphere. Then, a fast weight loss close to 68% for the catalyst and 90% for the support occurred from 400 to 700 °C [20]. Finally, the weight of the sample remained constant after 700 °C until 1000 °C. Nevertheless, for the untreated MWCNTs, weight loss was observed from the beginning until the end, being moderate–fast in the range 35–500 °C, high–fast between 500 to 700 °C and moderate–fast in the last range.

In this sense, the fast weight loss could be attributed to the oxidation of oxygenated surface groups, such as quinones or carboxyls, in the catalyst and support [23,27]. Moreover, a difference of weight loss of approximately 20% between the catalyst and the support after 700 °C was found that can be attributed to the experimental iron content in the prepared catalyst. From this observation, it could be suggested that the iron content in the Fe_3O_4 /MWCNTs catalyst remained constant along the cycles, and therefore, the activity of the solid could be considered unalterable. Furthermore, it could be concluded that the treatment with H_2O_2 is a practical method for the surface functionalization of MWCNTs.

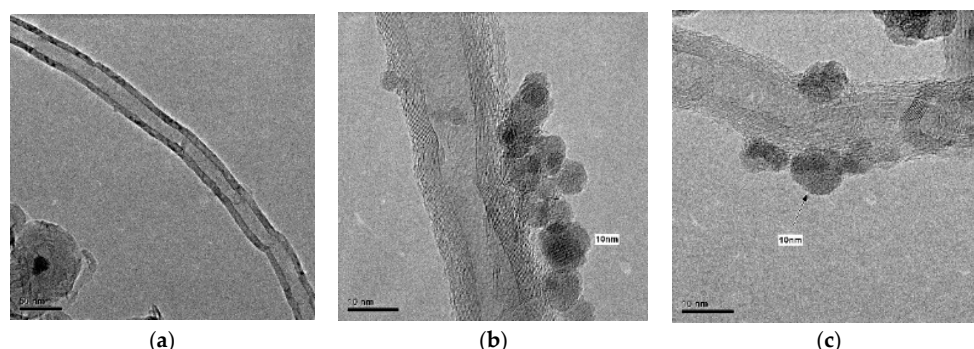


Figure 1. Cont.

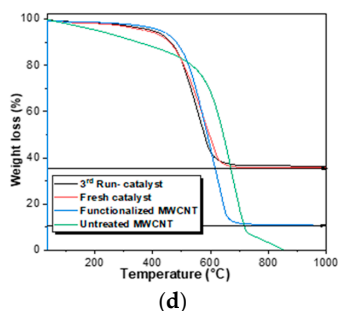


Figure 1. TEM micrographs of (a) functionalized multi-walled carbon nanotubes (MWCNTs), (b) magnetite/multi-walled carbon nanotubes ($\text{Fe}_3\text{O}_4/\text{MWCNTs}$), and (c) $\text{Fe}_3\text{O}_4/\text{MWCNTs}$ -2 (second reuse); (d) TGA of the untreated support, functionalized support, the fresh catalyst, and third reuse.

On the other hand, XRD patterns of the functionalized MWCNTs, the fresh catalyst, and the reused solids are shown in Figure S1 (Supplementary Material). According to the standard pattern of magnetite (JCPDS file No. 19-0629), the (220), (311), (400), (422), (511), and (440) planes of Fe_3O_4 could be observed.

FT-IR spectra determined the nature of the chemical groups in the untreated support (multiwalled carbon nanotubes-MWCNTs), the functionalized support, and the catalyst (fresh and reused) (Figure 2a). The absorption bands found at 3410 cm^{-1} correspond to the stretching mode of O–H. A peak at 2922 cm^{-1} observed in the spectrum of the support was assigned to the asymmetric and symmetric of C–H stretching vibration, considered defect sites of the MWCNTs. The band at 1740 cm^{-1} is attributed to C=O stretching vibrations and the peak observed at 1622 cm^{-1} was assigned to the stretching vibration of C=C double bonds. The band at 1054 cm^{-1} can be attributed to C–O and C–O–C stretching. Comparing the MWCNTs (treated and untreated) and the catalyst (fresh and reused), an additional peak at a wavelength of 568 cm^{-1} in the FTIR spectra of the catalyst could be found, resulting from the Fe–O stretching vibration of the Fe_3O_4 , suggesting the formation of the $\text{Fe}_3\text{O}_4/\text{MWCNTs}$ catalyst and the interaction between Fe_3O_4 and the functionalized MWCNTs [20,28]. Both similar bands at 568 cm^{-1} were observed in the fresh and reused catalysts, indicating that the solid maintained the load of magnetite on the MWCNTs after use.

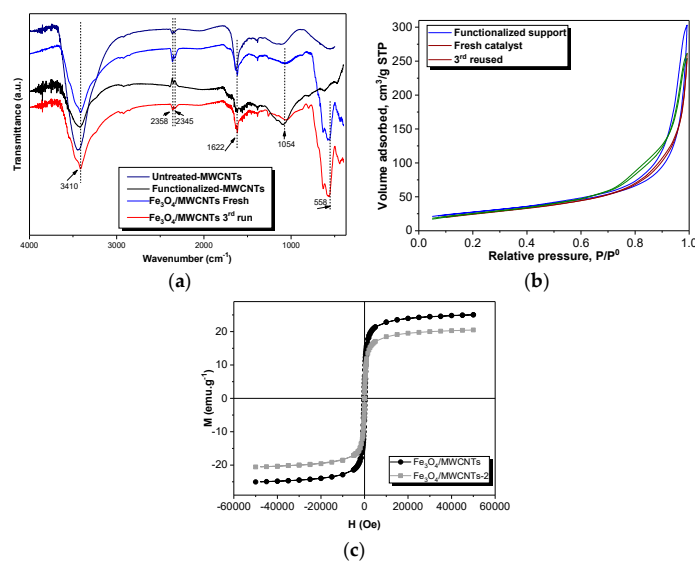


Figure 2. (a) FT-IR spectra of the untreated, functionalized support, and catalysts (fresh and reused); (b) N_2 adsorption–desorption isotherms at 77 K of the functionalized support and the catalyst (fresh and third reuse); (c) magnetization hysteresis loop of $\text{Fe}_3\text{O}_4/\text{MWCNTs}$ and $\text{Fe}_3\text{O}_4/\text{MWCNTs}$ -2 (second reuse).

Nitrogen adsorption–desorption experiments at 77 K were performed to analyze the textural properties of the catalyst. N₂ isotherms of the functionalized support, and the fresh and third-reused catalysts are depicted in Figure 2b. The isotherms of these materials followed type IVa adsorption isotherm according to IUPAC classification [29] that is usually found in mesoporous materials. The average values of specific surface area ($S_{\text{BET}} = 92.7 \text{ m}^2/\text{g}$), micropore volume ($V_{\text{Mic}} = 0.053 \text{ cm}^3/\text{g}$), total pore volume ($V_{\text{Total}} = 0.23 \text{ cm}^3/\text{g}$), and pore diameter (15.8 nm) could be determined due to the high similarity among the tested samples (Table 1). The Brunauer–Emmett–Teller (BET) surface area values, calculated by using the BET equation, ranged from $97 \text{ m}^2/\text{g}$, for the functionalized support to $90 \text{ m}^2/\text{g}$ for the fresh catalyst and $91 \text{ m}^2/\text{g}$ for the third-reused catalyst, suggesting that the textural properties of the reused catalyst did not change after the reaction.

Table 1. Textural properties of the materials.

Material	S_{BET} (m^2/g)	V_{Mic} (cm^3/g)	V_{Total} (cm^3/g)	$V_{\text{Mic}}/V_{\text{Total}}$	Average Pore Width (nm) *
Functionalized support	97	0.06	0.23	0.26	17.9
Fresh catalyst	90	0.05	0.23	0.21	14.7
3rd reused catalyst	91	0.05	0.23	0.21	14.7

* Average pore size at 4V/A by BET.

The magnetic properties of Fe₃O₄/MWCNTs and Fe₃O₄/MWCNTs-2 (second reuse) catalysts were evaluated by the accomplishment of the magnetization hysteresis curves. In Figure 2c is plotted the M–H hysteresis loop of the solids measured at the maximum external field of 60 kOe at ambient temperature. Both magnetization curves showed typical S-type hysteresis loops with no remanence or coercivity, illustrating the superparamagnetism of the samples. The saturation magnetization of the catalyst was found to be 25.0 emu/g, a similar value to that calculated for the second-reused catalyst (20.0 emu/g). According to Fan et al. [26], a saturation magnetization of 16.3 emu/g is enough to allow the magnetic separation of the catalyst from the solution by applying an external magnetic field, further confirming the good magnetic properties of both the fresh and reused catalysts.

The elemental analysis of the functionalized support, and the fresh and third-reused catalyst is collected in Table 1. The CHNS measurements revealed that %C in the fresh and third-reused catalysts was found to be very similar, indicating that the formation of carbonaceous deposits on the surface of the catalyst did not occur during the CWPO experiments. Additionally, the total iron content in the fresh catalyst, the third-reused catalyst, and the effluent of the third cycle was measured (Table 2). Since there was no detected iron content in the effluent of the reaction (no leaching of the active phase), the difference of 3% of Fe content observed in the fresh and third-reused catalysts can be considered as the error of the analytical measurement, attributed to a non-uniform distribution of the iron on the surface of MWCNTs.

Table 2. Elemental analysis of the functionalized support and the catalyst (fresh and third reuse).

	Fe%	% C	% H	% N	% S
Functionalized support	n.d.	84.47	0.77	0.19	0.00
Fresh catalyst	20.57	57.99	0.85	0.17	0.12
3rd reused catalyst	17.52	57.63	0.70	0.11	0.05
Effluent from 3rd reused catalyst	n.d.	n.d.	n.d.	n.d.	n.d.

n.d., not detected.

2.2. Effects of the Operating Variables on the Removal of NAP

The CWPO performance relative to the removal of NAP was evaluated with the variation of the different operating variables. The removal efficiency of NAP (η_N) determined at the steady state can

be defined by Equation (1), and it was calculated at several operation conditions (Table 3). The system variables include three-level incomplete factorial designs.

$$\eta_N = \frac{(C_{N0} - C_N)}{C_{N0}} \quad (1)$$

where C_{N0} and C_N are the concentrations of NAP (mg/L) at the initial time and any time t , respectively.

A quadratic polynomial response surface model was found to represent the relationship between NAP removal percentage and the independent input variables (See Equation (2)). Equation 2 ($R^2 = 0.995$) can be used to fit the experimental data obtained by the BBD model.

$$Y = 97.17 + 11.04A + 2.04B - 21.28C - 2.63A^2 - 0.18AB + 1.18AC - 0.002B^2 - 0.20CB + 1.25C^2 \quad (2)$$

where A , B , C , and Y are the initial H_2O_2 dosage (mM), temperature ($^{\circ}C$), pH, and NAP removal efficiency (%), respectively.

The obtained model (Equation (2)) explained the accuracy of the experiments and only 0.51% of the total variation cannot be explained, which ensures the goodness of the fit ($R^2 = 0.995$) [30]. The F value (131.32) and p -value (0.000003) with the estimated pure error of 0.5 and the predicted error variance of the model (2.29) indicated the validity of Equation (2) (See Table 4). The strong linear correlation between the experimental and the predicted values of NAP removal efficiency (Figure 3) demonstrated that the proposed model is accurate for investigating the effect of the three operation parameters.

All the terms of the model and significance of each term in the obtained regression model are listed in Table 5. The p -values of the model—quadratic interaction of temperature and individual coefficient of H_2O_2 dosage—are not significant because of $p = 0.05$, since all the other terms are significant, that means the predicted model mostly explains the probability of occurrence.

The uncertainty in the model predictions mainly depends on two major factors; one is the sample size and the other is the coefficients of the model. The sample size has been optimized with BBD, hence, there is a lesser scope of uncertainty. The other most important aspect leading to uncertainty is the coefficients of the model, in which insignificant model coefficients are present.

The model coefficients significance can be assessed using the p -test. The p -value of the overall F-test is affected by the p -values of the individual coefficients in the model. In this particular situation, the majority of individual coefficients have p -values that are significant except a quadratic interaction (B2) and an individual coefficient (A) (Table 5). Since the effect of B2 and A on the operating parameters is so small on the overall effect of the obtained model, these terms are negligible in the model prediction. Nevertheless, the model response predictions including those terms in the model equation were found so close to the experimental yields, and by the hierarchical principle of the regression model, B2 and A will remain in the final model [31,32].

The reported model showed an optimum NAP removal efficiency of 82.54%, whereas the experimental NAP removal percentage was found to be 82.00% (Table 3). Hence the predictions of the regression model using the response surface Methodology (RSM) showed an average value of deviation of 2% with the experimental results. Due to the very small value of deviation, it could be concluded that the prediction of the developed model showed a high accuracy.

2.3. Reaction Kinetics and Activation Energy Determination

The CWPO experiments of NAP were performed at different temperatures (30, 50, and 70 $^{\circ}C$), maintaining constant the values of H_2O_2 dosage (1.5 mM), pH (5), and catalyst dose (1 g/L). All the experiments were accomplished during 3 h reaction time. It is noteworthy to say that the pH did not change at the end of the reaction.

Firstly, the initial reaction rate (k_0 , mmol/min·g_{cat}) values were calculated at the tested temperatures, resulting in 2.67×10^{-3} , 3.48×10^{-3} , and 3.99×10^{-3} mmol/min·g_{cat} for 30, 50, and 70 °C, respectively (Table 6). Thus, as expected, the temperature showed a significant effect on the oxidative process of NAP, increasing the initial reaction rate.

Table 3. Experimental design matrix of the degradation of naproxen (NAP) by catalytic wet peroxide oxidation (CWPO).

Run	Actual Values			NAP Removal Efficiency (%)		
	A (H ₂ O ₂ dosage) (mM)	B (Temperature) (°C)	C (Initial pH)	Observed	Predicted	Error
1	1.5	70	5	82.00	82.54	−0.54
2	2.5	50	5	71.72	70.25	1.46
3	1.5	70	9	16.94	17.77	−0.83
4	2.5	70	7	40.00	40.92	−0.92
5	1.5	30	5	62.70	61.86	0.83
6	0.5	70	7	46.44	44.14	2.29
7	2.5	50	9	28.14	26.38	1.75
8	1.5	50	7	45.00	43.85	1.14
9	1.5	50	7	43.74	43.85	−0.11
10	1.5	50	7	43.60	43.85	−0.25
11	1.5	50	7	43.07	43.85	−0.78
12	0.5	50	5	69.00	70.75	−1.75
13	0.5	30	7	33.14	32.21	0.92
14	2.5	30	7	41.55	43.85	−2.29
15	0.5	50	9	16.00	17.46	−1.46
16	1.5	30	9	30.00	29.46	0.54

Reaction conditions: [NAP]₀ = 10.0 mg/L, [catalyst] = 1.0 g/L, atmospheric pressure, 3 h reaction time.

Table 4. Analysis of variance (ANOVA) of the quadratic polynomial model.

	df	SS	MS	F	Prob > F (p-Value)
Regression	9	5266.87	585.21	131.32	0.000003
Residual	6	26.74	4.45		
Total	15	5293.61			

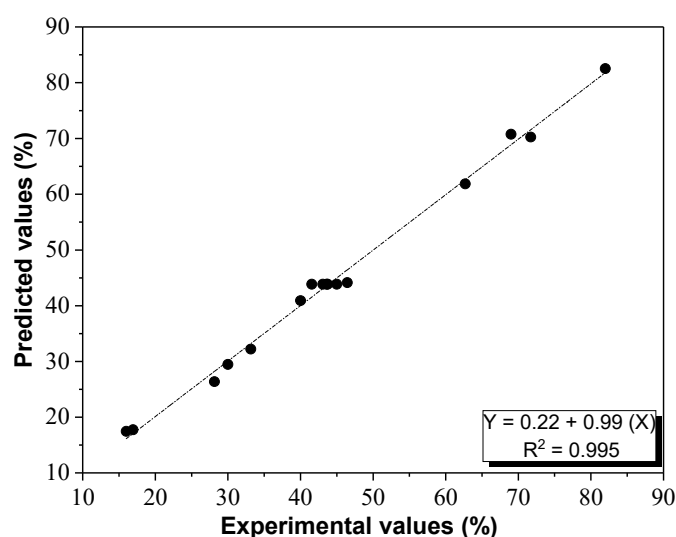


Figure 3. Linear correlation between the experimental and the predicted values of NAP removal efficiency.

Table 5. *p*-test significance of model terms in the quadratic polynomial model.

Model	Model Coefficient	Coefficient Estimate	Standard Error	T Stat	<i>p</i> Value	Degree of Significance
Intercept	β0	97.17	18.37	5.29	0.002	Significant
A-Per	β1	11.04	5.58	1.97	0.095	Not significant
B-Tem	β2	2.04	0.33	6.11	0.001	Significant
C-pH	β3	−21.28	4.01	−5.29	0.002	Significant
AB	β12	−0.19	0.05	−3.52	0.013	Significant
BC	β23	−0.20	0.03	−7.66	0.000	Significant
CA	β13	1.17	0.53	2.23	0.067	Possibly significant
A ²	β11	−2.63	1.05	−2.49	0.047	Significant
B ²	β22	−0.002	0.003	−0.89	0.409	Not significant
C ²	β33	1.25	0.26	4.73	0.003	Significant

Table 6. Initial reaction rate values for CWPO of NAP at different temperatures.

Temperature (°C)	30	50	70
k_0 (mmol/min·g _{cat}) × 10 ³	2.69	3.54	3.99
R ²	0.964	0.983	0.961

Reaction conditions: [NAP]₀ = 10.0 mg/L, pH = 5.0, [catalyst] = 1.0 g/L, [H₂O₂]₀ = 1.5 mM, 3 h reaction time.

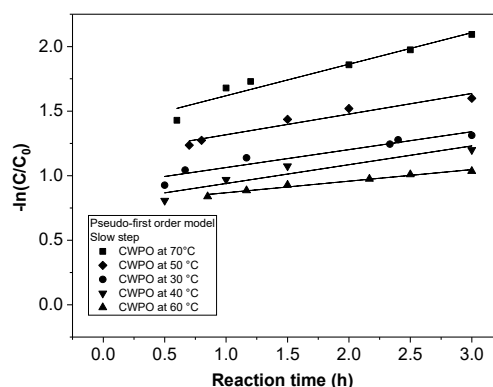
Secondly, the kinetic-order reaction of NAP removal by the synthesized catalyst in CWPO at the different tested temperatures has been discussed. The transformation of NAP to carbon dioxide and water can also be expressed in a single step as it is shown in Equation (3):



The obtained data from NAP removal by CWPO were used to find a suitable law rate that describes the reaction rate in the process. As it has been reported in the literature [33], the catalytic reaction of any organic compounds in the presence of a large excess of hydrogen peroxide, compared to the stoichiometric amount, follows a pseudo-first-order law, described in Equation (4).

$$-\ln\left(\frac{C}{C_0}\right) = k.t \quad (4)$$

where C_0 and C (mol/L) are the molar concentrations of NAP at the initial time and any time t , respectively, while k (h^{-1}) is the apparent pseudo-first-order rate constant. From Equation (4), the plot $\ln(C_0/C)$ versus time (Figure 4) depicts the NAP degradation profiles at the different tested temperatures, where only the slow stage of the reaction has been plotted. The apparent pseudo-first-order rate constants were estimated from the slope of the straight lines as a function of the temperature. The rate constants and the obtained regression coefficients (R^2) are shown in Table 7. From the obtained values of R^2 , it could be concluded that the pseudo-first-order equation did not satisfactorily fit the experimental data [34,35].

**Figure 4.** $-\ln(C/C_0)$ versus reaction time plot at different temperatures.

Thirdly, the kinetic evolution of NAP removal by using the $\text{Fe}_3\text{O}_4/\text{MWCNTs}$ catalyst in CWPO was also fitted to the pseudo-second-order kinetic model [33]. Hence, as it has been reported by Haji et al. [33], the pseudo-second-order model can usually be considered most suitable to describe the experimental data of azo dyes treated by CWPO. This model equation can be described by Equation (5) and its integrated form at a constant-density batch reactor is defined by the Equation (6):

$$-r = k(C - C^*)^2 \quad (5)$$

$$C = C^* + \frac{1}{\frac{1}{C_0 - C^*} + kt} \quad (6)$$

where k (L/mg·h) is the pseudo-second-order rate constant and C^* (mg/L) is the minimum concentration of the pollutant in the aqueous solution. Since the resulting equation cannot be linearized, a nonlinear regression analysis was used to estimate k and C^* values (Table 7); thus, the experimental and predicted data are depicted in Figure 5a. As it can be seen, the pseudo-second-order model successfully described the experimental data. So, the estimated apparent rate constants were 0.80, 0.85, 0.91, 0.96, and 0.99 L/mg·h for 30, 40, 50, 60, and 70 °C, respectively. These values are higher than that reported by Haji et al. [33] in the treatment of an azo dye (0.36 L/mg·h).

The activation energy (E_a) and frequency factor (A) of NAP removal was calculated from the Arrhenius equation (Figure 5b), and the obtained values were 4.75 KJ/mol and 5.29 h^{-1} , respectively. The estimated E_a value for CWPO of NAP is lower than the activation energy associated to an adsorption processes, e.g., 37.3 KJ/mol for NAP adsorption onto activated carbon [36].

2.4. Effect of the Operating Parameters on CWPO: Response Surface Methodology Technique

In the present study, the optimization of NAP removal by CWPO through the Box–Behnken Design (BBD) and RSM model was accomplished. The maximum NAP removal was found at a temperature of 70 °C, a H_2O_2 dosage of 1.5 mM, and pH of 5; thus, the effect of the operation parameters on NAP removal was highlighted in RSM plots shown in Figure 6a–d. Predicting response outside of the range of the independent variables may not give accurate results since the change of the independent variable range led to a change in the intercept and coefficients of the developed regression model. For the original design of experiments and optimization, regression models were developed by considering the range of independent variables, such as temperature, hydrogen peroxide dosage, and pH, from previous studies of diclofenac removal by CWPO. Reasons behind the optimum removal at these conditions from the obtained mathematical models, and relevant experimental and predicted observations are listed below.

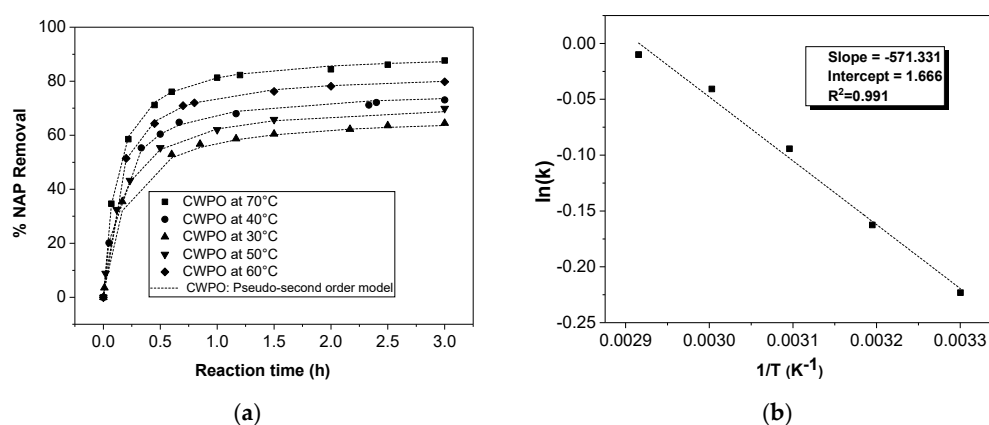


Figure 5. (a) Modeling of experimental data by pseudo-second-order kinetic model (at five different temperatures); (b) Arrhenius plot for CWPO experiments of NAP ($[\text{NAP}]_0 = 10.0 \text{ mg/L}$, $\text{pH} = 5.0$, $[\text{catalyst}] = 1.0 \text{ g/L}$, $[\text{H}_2\text{O}_2]_0 = 1.5 \text{ mM}$).

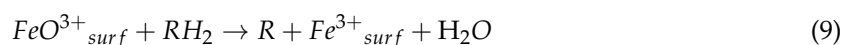
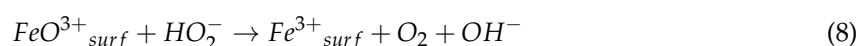
Table 7. Kinetics parameters for the degradation of NAP at different temperatures for pseudo-first-order and pseudo-second-order models.

T (°C)	Pseudo-First-Order Model ¹		Pseudo-Second-Order Model ¹		
	Slow Step k_2 (h ⁻¹)	R ²	C* (mg/L)	k (L/mg·h)	R ²
30	0.11	0.924	3.18	0.80	0.999
40	0.14	0.891	2.70	0.85	0.999
50	0.11	0.972	2.35	0.91	0.998
60	0.16	0.938	1.70	0.96	0.999
70	0.29	0.899	0.96	0.99	0.999

¹ Reaction conditions: [NAP]₀ = 10.0 mg/L, pH = 5.0, [catalyst] = 1.0 g/L, [H₂O₂]₀ = 1.5 mM, 3 h reaction time.

2.4.1. Combined Effect of Hydrogen Peroxide Dose and pH on NAP Removal

The efficiency of hydrogen peroxide is one of the parameters that requires optimization in CWPO processes. The hydrogen peroxide and catalyst are critical parameters which determine the optimal production and consumption of the generated hydroxyl radicals; thus, for example, the use of optimal doses will reduce the formation of parasitic reactions (Equations (7)–(9), (11)–(14)) and the generation of oxygen and water [37]. The stoichiometry of the reaction clearly indicates that only 32 moles of hydrogen peroxide is typically required for one mole of NAP; however, the catalytic reaction for degradation of NAP requires an extra amount of hydrogen peroxide in order to shift the equilibrium towards CO₂ and H₂O formation.



In this case, the effect of hydrogen peroxide concentration within the range from 0.5 to 2.5 mM for a mmol of NAP at different pH values (5–9) has been explored (Figure 6a). Figure 6a indicated that maintaining all the other operation parameters constant, a decrease in the pH solution (from 9 to 5) enhanced the NAP removal up to 60.0%, due to the promotion of the •OH formation. In contrast, in alkaline solution, H₂O₂ is decomposed in water and oxygen, and therefore the amount of •OH radicals produced during the reaction will be reduced. This trend was observed for the whole range of the studied H₂O₂ concentrations. On the other hand, overall experiments also revealed that the optimum value of hydrogen peroxide concentration for a mmol of NAP was 1.5 mM at pH 5. Thus, the evolution of hydrogen peroxide efficiency (η) upon reaction time at 30 °C and pH = 5–9 is depicted in Figure 7, where a favorable effect in H₂O₂ efficiency was observed at acidic pH values. At these conditions, the efficiency of H₂O₂ showed its maximum ($\eta = 1$ mg/mg at 10 min for pH 5) and decreased up to around 0.50 mg/mg as mineralization proceeded within 3 h reaction time. At neutral pH, the efficiency of H₂O₂ achieved its maximum from 10 to 30 min, and then it started to decrease until approximately 0.30 mg/mg. On the other hand, at pH 9, a dramatic decrease in the H₂O₂ efficiency was observed, which could be attributed to the instability of H₂O₂ in alkaline medium. It has been observed that, at these conditions, the decomposition of H₂O₂ occurred as H₂O and O₂ instead via formation of hydroxyl radicals [38,39].

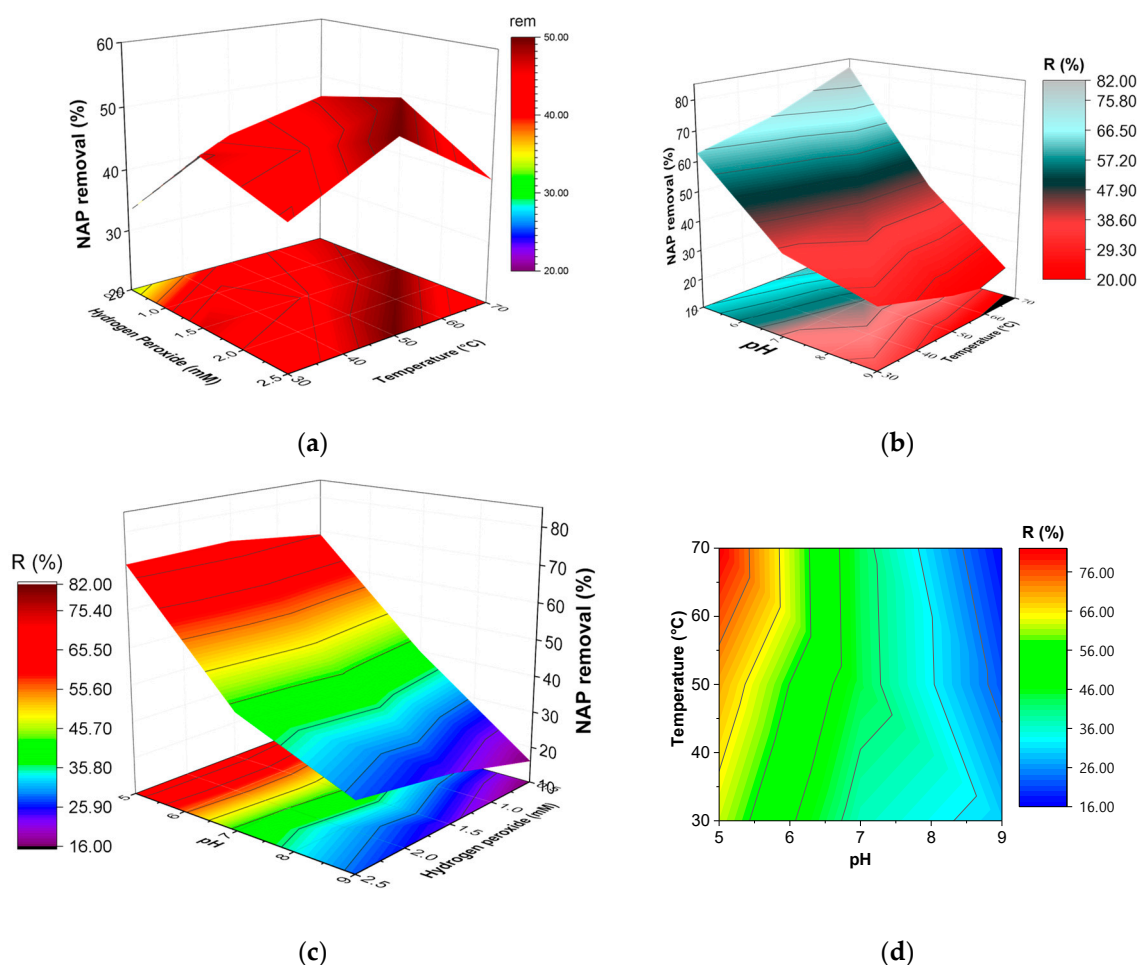


Figure 6. Combined effect of (a) H_2O_2 vs. temperature, (b) H_2O_2 vs. pH, and (c) pH vs. temperature on the NAP removal; (d) contour plot of temperature and pH on the NAP removal.

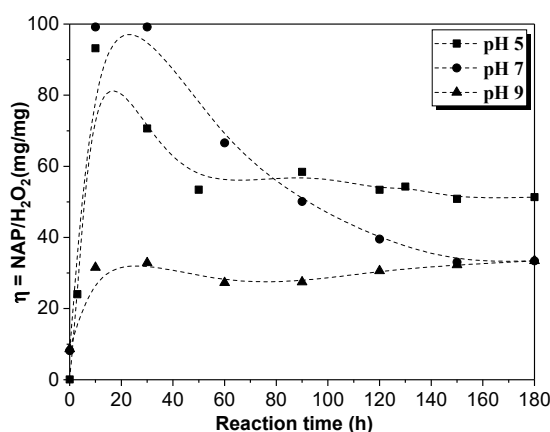


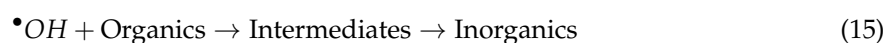
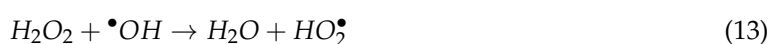
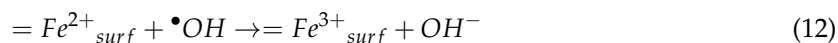
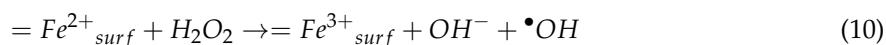
Figure 7. Effect of initial pH on the efficiency of H_2O_2 . Reaction conditions: $[\text{NAP}]_0 = 10 \text{ mg/L}$, $\text{pH} = 5$, $[\text{catalyst}] = 1.0 \text{ g/L}$, $[\text{H}_2\text{O}_2]_0 = 1.5 \text{ mM}$, $T = 30 \text{ }^\circ\text{C}$.

2.4.2. Effect of Temperature

In the current work, overall experiments were carried out at a temperature range of 30–70 °C and a H_2O_2 dosage ranging from 0.5 to 2.5 mM along 3 h reaction time. The effect of the interaction between the reaction temperature and hydrogen peroxide concentration on NAP removal is shown in Figure 6b. Generally, an increase in the H_2O_2 dosage can enhance the NAP removal due to the

favoring of $\bullet\text{OH}$ formation, since the H_2O_2 dose in excess would act as a scavenger of $\bullet\text{OH}$ radicals, as it is shown in Equations (12)–(14) [37]. In this work, the maximum NAP removal value was found to be 82% using a H_2O_2 dosage of 1.5 mM and a temperature of 70 °C.

According to the literature [40], the H_2O_2 dosage should have an appropriate range in the heterogeneous Fenton process for an efficient generation of hydroxyl radicals ($\bullet\text{OH}$). The common reactions that occur in the Fenton process can be described as follows:



In this particular case, the excess in the H_2O_2 concentration led to a decrease in the degradation of NAP. This is attributed to the generation of secondary reactions that usually occur, such as the reaction of $\bullet\text{OH}$ with H_2O_2 and the reaction of two molecules of $\bullet\text{OH}$ (Equations (13) and (14)).

On the other hand, when the H_2O_2 dosage was deficient (0.5 mM), the removal of NAP also showed a dramatic decrease due to the oxidizing agent ($\bullet\text{OH}$) concentration in the reaction not being enough. These results are in good agreement with the results obtained by Wang et al. [41].

Figure 6c,d shows the combined effect between temperature and pH on the removal efficiency of NAP. It could be concluded that an increase in the operating temperature, combined with a low pH value, led to a high enhancement of the NAP removal.

2.5. Catalyst Stability

For the heterogeneous CWPO process, the reusability and stability of the catalyst is a main aspect to be considered in the implementation of the technology. The results in this study revealed that pH had a remarkable effect in the reaction medium, due to the reaction of iron oxide on the surface of MWCNTs with H^+ ions in solution. Considering the fact that the catalytic activity mainly comes from the Fe element [42], the leached iron from the surface of the catalyst will definitely affect its reusability and stability and then, inevitably, it will further affect the treatment efficiency.

The reusability of the catalyst was evaluated under the following reaction conditions: $[\text{catalyst}] = 1.0 \text{ g/L}$, $[\text{H}_2\text{O}_2]_0 = 1.5 \text{ mM}$, $[\text{NAP}]_0 = 10 \text{ mg/L}$, $\text{pH} = 5.0$, and $T = 50 \text{ }^\circ\text{C}$. The catalytic behavior of the synthesized catalyst was tested along three consecutive experimental runs. As it is shown in Figure 8, the removal efficiency of NAP was close to 80% for the three cycles at pH 5, indicating that the solid maintained unalterable catalytic activity. Furthermore, the total iron content measured in the final effluent was negligible (Table 2). Thus, the catalyst can be considered as a stable material at pH 5 during the three runs of application. In addition, in order to evaluate the contribution of the support (MWCNTs) in the degradation of the pollutant, an adsorption test was accomplished, finding that the removal of NAP attributed to the adsorption onto the multi-walled carbon nanotubes surface was only about 5%. Additionally, the evolution of the H_2O_2 concentration was evaluated (Figure S2 of Supplementary Material), observing that the H_2O_2 consumption was similar in the three consecutive runs.

The synthesized catalyst showed similar values of stability as those found for the catalysts used by Cleveland et al. [42] that could be reused three times as well. The three CWPO experimental runs did not contribute to the loss of active sites displayed in the form of Fe_3O_4 on the surface of MWCNTs, but these still need to be further studied along more than three experimental runs.

A comparison between different iron-based catalytic systems for the removal of NAP in liquid phase is collected in Table S1 (Supplementary Material). From the results, it could be concluded that this solid is comparatively active and robust as the other iron-based systems found in the literature under similar NAP initial concentrations. Apart from that, this catalyst showed to be recyclable after three cycles of reaction at near neutral pH, no leaching was observed, and an easy separation from the liquid by its magnetic properties was accomplished.

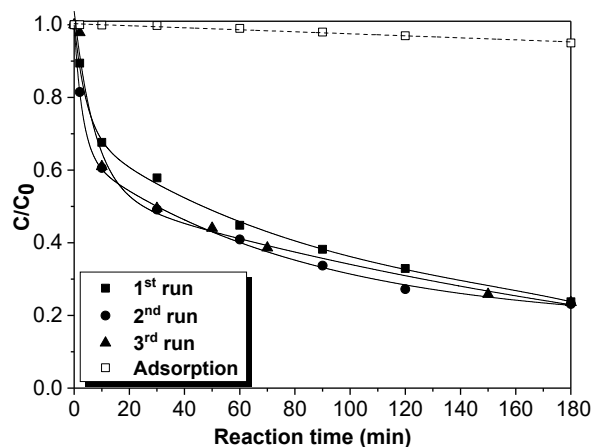


Figure 8. Performance of the catalyst upon three sequential runs of NAP removal by CPWO. Reaction conditions: $[NAP]_0 = 10 \text{ mg/L}$, $\text{pH} = 5$, $[\text{catalyst}] = 1.0 \text{ g/L}$, $[\text{H}_2\text{O}_2]_0 = 2.5 \text{ mM}$, $T = 70 \text{ }^\circ\text{C}$.

2.6. Quenching Test of Hydroxyl Radicals

The generation of $\bullet\text{OH}$ radicals in the CWPO system was firstly investigated by adding 2-propanol and n-butanol as $\bullet\text{OH}$ scavengers. As it is shown in Figure S3 (Supplementary Material), the addition of n-butanol significantly decreased the NAP removal efficiency, suggesting that $\bullet\text{OH}$ radicals were the main reactive species existing in this system. Furthermore, 2-propanol was added to the system, showing an additional reduction of the NAP removal.

2.7. Reaction Mechanism

An aliquot of the treated NAP sample was collected after 3 h reaction time and was analyzed by (–)-ESI-LC-MS technique using NAP as standard. A total of 26 peaks (Figure S4 of Supplementary Material) were detected for the sample compared to seven peaks observed for NAP standard (naproxen $M = \text{C}_{14}\text{H}_{13}\text{O}_3$; molecular weight = 229 g/mol; $t_R = 20.2 \text{ min}$) (Figure S5 of Supplementary Material). The detected ions corresponding to the degradation products of NAP in ultrapure water ((–)-ESI m/z 217, 231, 230, 187, 185, 201, 177 and 209) were collected in Table S2. Thus, the possible degradation pathways based on the identified degradation byproducts are presented in Figure 9. According to the results of the scavenging tests, the removal of NAP in the studied system was mainly due the $\bullet\text{OH}$ radicals attack [43]. Thus, the formation of the Cs may be attributed to the rapid attack of $\bullet\text{OH}$ via hydroxylation process (C1, C3, A, C8, C9, and B), which is a common reaction pathway in $\bullet\text{OH}$ reactions of aromatic molecules [43], with the subsequent demethoxylation (C1 and C8) or decarboxylation (C5, C6). Irrespective of the CWPO reaction mechanism of NAP, the three major detected intermediates were C4 (carboxylate NAP (m/z 229)), C5 (1-ethyl-6-methoxynaphthalene (m/z 187)), and C6 (2-Methoxy-6-vinylnaphthalene (m/z 185)).

In route A, the demethoxylation of NAP by $\bullet\text{OH}$ radicals attack led to the formation of the C1 compound (2-(6-Hydroxy-2-naphthyl) propanoic acid) [43]. The analysis also detected the presence of an ion (C3) that could be a rearrangement resulting from a demethylation of the methoxy functionality and an incorporation of the methyl onto the naphthalene ring.

In route B, carboxylate NAP was converted to the corresponding carboxyl radical by $\bullet\text{OH}$ reaction and the subsequent decarboxylation yielded C5 intermediate. The compound C5 has been detected by Kanakaraju et al. [44] as well. The abstraction of hydrogen of C5 yielded C6 and the attack of $\bullet\text{OH}$ in the vinyl group (C6) resulted in the formation of A (not detected) and C7 (2-Acetyl-6-methoxynaphthalene) [43,44]. Sequentially, the demethoxylation of A (1-(6-Methoxynaphthalen-2-yl) ethylhydroperoxide) by the attack of $\bullet\text{OH}$ and the subsequent carboxylation and decarboxylation yielded C8 (naphthalene-1,3,7-triol) and C9 (naphthalene-1,2,3,4,6-pentaol) [45]. B (2-hydroxy-3-oxo succinic acid) was produced by the opening of the ring after several attacks of $\bullet\text{OH}$ radicals. These intermediates were also reported in the literature as the most common NAP degradation byproducts by $\bullet\text{OH}$ -based oxidation processes [43,45].

It should be taken into account that the concentration of the intermediates was analyzed at the end of 3 h reaction time, where the detection limit had declined to below after destruction of NAP molecule.

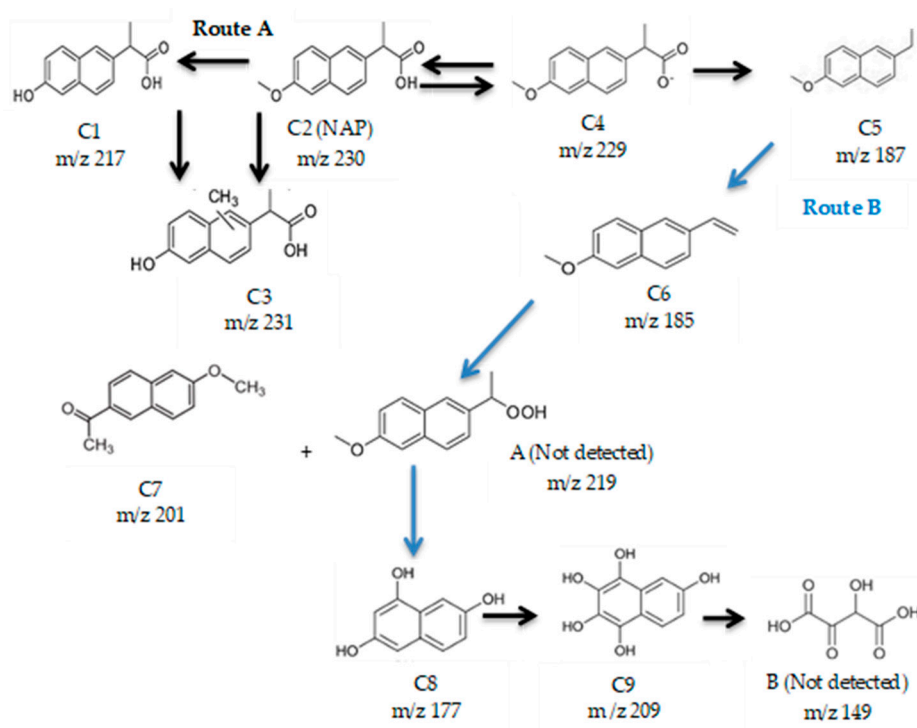


Figure 9. Proposed reaction pathways for the degradation of NAP by CWPO.

2.8. Catalytic Wet Peroxide Oxidation in Different Real-Aqueous Matrices

The chemical oxidation of different aqueous matrices, e.g., a surface water (NAP-SW), a hospital wastewater (NAP-HW), and a wastewater treatment plant effluent (NAP-WWTP) spiked with NAP was performed at the optimum CWPO conditions. All the experiments were conducted using 1 g/L of catalyst, 10 mg/L of the pollutant, at 70 °C, and pH of 5 for 8 h reaction time. In each experiment, the TOC concentration, the aromatic content (A_{254}), pH, total nitrogen (TN) concentration, H_2O_2 concentration, and NAP concentration were determined at regular times. The evolution of TOC, TN, H_2O_2 concentrations, and the efficiency of H_2O_2 versus reaction time for the tested aqueous matrices is depicted in Figure 10a–d. Figure 10c showed the degradation of TOC versus reaction time and the efficiency of H_2O_2 .

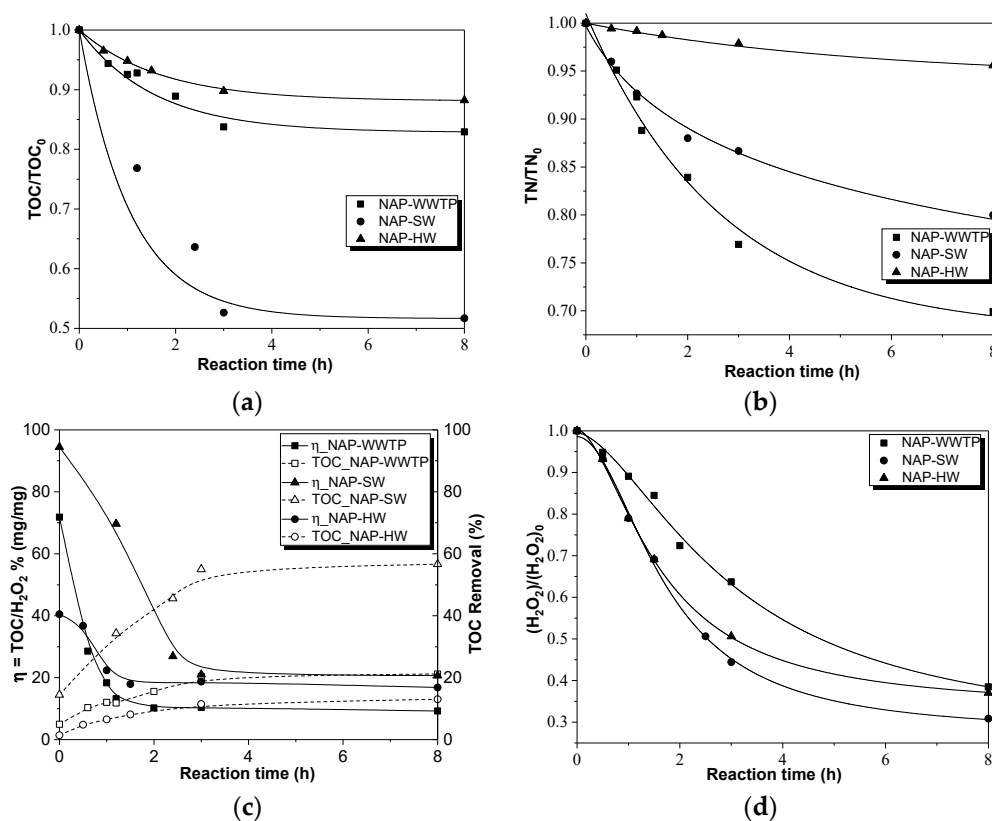


Figure 10. Degradation of the aqueous matrices spiked with NAP by CWPO; (a) evolution of total organic carbon (TOC) concentration; (b) evolution of total nitrogen (TN) concentration; (c) evolution of efficiency of hydrogen peroxide to TOC; (d) evolution of H₂O₂ concentration. Reaction conditions: [NAP]₀ = 10 mg/L, pH = 5, [catalyst] = 1.0 g/L, [H₂O₂]₀ = 1.5 mM, T = 70 °C.

At the operating conditions, for NAP-HW and NAP-WWTP samples, only 10% and 15% of TOC removal, respectively, could be achieved. Meanwhile, for the NAP-SW matrix, the removal of TOC was found higher (50%), maybe due to the low initial TOC value of the surface water (6.8 mg/L) (See Table S3 of Supplementary Material). In addition, the pH values measured after 8 h reaction time for NAP-SW, NAP-HW, and NAP-WWTP samples were 3.98, 6.5, and 5.5, respectively. So, for the NAP-SW sample, the pH in the reaction medium decreased from 5 (initial pH) to 3.98; for NAP-HW, the pH increased 1.5 units, and it was maintained constant (5.5) in the case of the NAP-WWTP matrix. From those results, it could be suggested that the effect matrix is playing a main role in the CWPO process of NAP [46].

On the other hand, the removal of TN in the NAP-HW sample was only about 5%, while for NAP-SW and NAP-WWTP matrices it was slightly higher, at 20% and 30%, respectively (Figure 10b). From the obtained results, it could be concluded that the organic matter present in the HW and WWTP samples can act as a scavenger of •OH radicals in the CWPO reaction [47].

The evolution of H₂O₂ efficiency of the tested aqueous matrices spiked with NAP is depicted in Figure 10c. As it can be seen in Figure 10c, the efficiency of H₂O₂ changed along the reaction time. In the case of NAP-SW effluent, during the first seconds of the reaction, the efficiency achieved 0.98 mg/mg and then it started to decrease until it reached 0.20 mg/mg at 2.5 h reaction time, maintaining this value until the end of the reaction. A similar behavior was observed for NAP-HW and NAP-WWTP samples, with lower efficiencies achieved in the first stage of the process. These values are in accordance to the measured TOC removal values.

Similarly, the evolution of the aromaticity content along the reaction was depicted for the three tested aqueous matrices, observing removal values ranging from 25% to 50% (Figure S6a of Supplementary Material). The highest reduction was observed for the surface water (SW) effluent (50%), in comparison to 25% and 35%, obtained for HW and WWTP effluent, respectively. These results are in agreement with those obtained by Benitez et al. [48].

Since the highest removal of the aromatic content was found for the NAP-SW sample, the effect of the presence of the pollutant in the SW sample was evaluated at the same operation conditions (Figure S6b of Supplementary Material). As it can be seen, the absorbance ($A_{254\text{ nm}}$) of the surface water dramatically decreased (up to 95%) in comparison to the sample spiked with naproxen (NAP-SW). So, it could be suggested that the extra recalcitrant organic matter attributed to the micropollutant had a detrimental effect on the degradation of the aromatic compounds, if the dose of H_2O_2 in excess referred to the stoichiometric amount. So, it could be concluded that the more recalcitrant or complex organic matter consumes an important amount of H_2O_2 in the CWPO reaction before the removal of the more readily degradable organic matter occurs [47].

Toxicity Evaluation

The ecotoxicity of the effluent is an interesting fact to test the efficiency of the CWPO technology. Since, usually, wastewater matrices have been reported to contain several recalcitrant and toxic compounds in which are included the pharmaceutical compounds like naproxen [1,4], the ecotoxicity is an important parameter due to its risk associated to the water environment and deserves to be measured after the treatment of real-aqueous matrices.

The ecotoxicity evaluation of the influent and effluent of the real wastewater matrices spiked with NAP after 8 h reaction time by CWPO process were assessed using a *Vibrio Fischeri* test [49].

Six ecotoxicity tests were accomplished for the three real wastewater matrices, and each test always had the same number of duplicated concentrations and a duplicated control treatment. Statistical analyses on the Microtox Data were performed using Microtox software[®], and the results were expressed as toxicity units (TUs) after 5 min of exposure.

The highest ecotoxicity value (TU = 6.1) was found for the influent NAP-WWTP sample, and NAP-SW and NAP-HW samples showed high values too (TU = 4.1 and 5.7, respectively). As it can be observed in Table 8, CWPO technology led to an outstanding decrease in the ecotoxicity values for the three real water matrices; specifically, one of the most critical cases—hospital wastewater—achieved a reduction of about 96.5%. Thus, for the three cases, the toxicity of the effluent remained at an acceptable value. The reduction of the toxicity was directly related to the non-presence of trace amounts of H_2O_2 , or the formation of toxic byproducts along the reaction [50].

So, the classification of toxicity of the three tested effluents resulted as follows: NAP-HW (no toxicity) > SW (no toxicity) > WWTP (medium–low toxicity) [51,52]. As it can be seen from the results, the catalyst used in the CWPO process depicted a clearly advantageous and environmentally friendly technology for the treatment of ecotoxic real-aqueous matrices.

Table 8. Toxicity values of the tested real-aqueous matrices.

Toxicity Units (TUs)			
	Influent	Effluent	Toxicity Class
NAP-WWTP	6.1	1.6	Medium-low toxicity
NAP-SW	4.1	0.8	No toxicity
NAP-HW	5.7	0.2	No toxicity

3. Materials and Methods

3.1. Materials

Multi-walled carbon nanotubes (MWCNTs) (diameter of 30–50 nm; length of 20 mm) were supplied by Sun Nanotech Co. Ltd. in Beijing, China. $\text{FeCl}_3 \cdot 6\text{H}_2\text{O}$, $\text{FeCl}_2 \cdot 4\text{H}_2\text{O}$, ammonia solution 25%, and H_2O_2 solution 30% (*w/w*) were purchased from Sigma-Aldrich (Overijse, Belgium). Naproxen (NAP) as sodium salt with a purity of more than 98% was purchased from Sigma-Aldrich. All the solutions used in the experiments were prepared in ultrapure water. Furthermore, a mini magnetic stirrer with plastic cover and an Aitsite magnet NFD 60 for the separation of the solid after reaction were acquired.

3.2. Synthesis of the Catalyst

3.2.1. Functionalization of the Support (MWCNTs)

An oxidative treatment of MWCNTs was carried out by using H_2O_2 as the oxidizing agent [53]. According to the method of Singer et al. [53] with some modifications, a solution of H_2O_2 18% (*w/w*) was used to dissolve 2.0 g of MWCNTs. Then, the suspension was heated at 80 °C for 4 h and, after, was thoroughly filtered and washed with ultrapure water until the washing water reached neutral pH. The material obtained was dried in an oven at 100 °C for 10 h.

3.2.2. Preparation of the Catalyst (Fe_3O_4 /MWCNTs)

The catalyst preparation was accomplished following the combination of two methods (co-precipitation and hydrothermal treatment) [23], with some modifications in the composition of the catalyst. Briefly, 120 mL of ultrapure water containing 0.20 g of MWCNTs was vigorously stirred at 60 °C in a three-neck flask under the purge of nitrogen gas. Then, 0.28 g of $\text{FeCl}_3 \cdot 6\text{H}_2\text{O}$, 0.08 g of $\text{FeCl}_2 \cdot 4\text{H}_2\text{O}$, and 0.5 mL of ammonia solution (25%) were added. After stirring for 30 min, the Fe_3O_4 /MWCNTs colloidal solution was formed. The obtained colloidal solution was transferred and sealed into a Teflon-lined autoclave reactor and then kept at 120 °C for 12 h. After, the precipitate was separated from the aqueous liquid by a magnet and then washed with ultrapure water until the washing water reached a pH value of 6.3. Finally, the formed solid of Fe_3O_4 /MWCNTs nanocomposites were ultra-sonicated for 3 min. Then, they were dried in a vacuum oven at 60 °C for 24 h.

3.2.3. Support and Catalyst Characterization

The morphology of the catalyst and the distribution of the magnetic nanoparticles supported on the MWCNTs were studied using transmission electron microscope (TEM, JEOL 3000F, Peabody, MA, USA). The thermogravimetric analyses were carried out in a thermal analyzer TGA Q500 (STA 6000, PerkinElmer, Waltham, MA, USA) under air atmosphere, following a heating rate of 10 °C min^{-1} from 30 to 1000 °C. The Fourier-transform infrared spectra were recorded in a Thermo Nicolet F-TIR spectrophotometer (Thermo Fisher Scientific, Waltham, MA, USA), in a wavelength range from 400 to 4000 cm^{-1} . The porosity of the materials was studied by N_2 adsorption–desorption isotherms at 77 K in an ASAP 2020 apparatus, with the samples outgassed for 3 h at 250 °C before the measurement. The specific surface area of the solids (S_{BET}) was calculated using the Brunauer–Emmett–Teller (BET) equation and the micropore volume (V_{Mic}) was estimated by using Dubinin–Radushkevich equation. The elemental microanalysis was accomplished in a LECO CHNS-932 analyzer (Leco Corporation, St. Joseph, MI, USA), where 0.6–1.6 mg of sample was held in a combustion furnace at 1000 °C. The magnetic properties of the solids were determined in a MPMS 5S superconducting quantum interference device (SQUID, San Diego, CA, USA). The total iron content of the samples was measured by wavelength dispersive X-ray fluorescence analysis (WDXRF), using an Axiom spectrometer (PANalytical) equipped with a Rh anode X-ray tube and maximum power of 4 kW.

3.3. Catalytic Wet Peroxide Oxidation (CWPO) Tests

A typical-batch CWPO experiment was carried out in a three-neck round-bottom flask using magnetic stirring, where 130 mL of NAP solution ($C_0 = 10$ mg/L) was added. The reactor had a reflux condenser and was maintained at a constant temperature using a thermostatic bath. pH was adjusted to the required value (with 1 M sulfuric acid solution) after the solution reached the reaction temperature; then, 0.13 g of catalyst, and immediately after, the required H_2O_2 dose were added, with time considered as zero for the catalytic reaction. At regular time intervals, samples were collected from the reactor and immediately filtered through a $0.45 \mu\text{m}$ PTFE filter.

When the CWPO experiment finished, the catalyst was separated from the reaction medium by the action of a magnet and the treated effluent was filtrated. The catalyst was washed several times with ultrapure water and dried before being used in the next cycle. The reusability of the catalyst was investigated during 3 consecutive tests at 50°C , 2.5 mM of H_2O_2 dose, and 1.0 g/L of catalyst.

3.4. Statistical Analysis through Response Surface Methodology: Box–Behnken Design

In this work, the effect of the operation parameters on the catalytic degradation of NAP was investigated. The statistical design was carried out by testing three factors—temperature, initial pH, and H_2O_2 dose, in order to determine the optimum removal of NAP. In the experiments, the catalyst concentration was maintained constant in a value of 1 g/L, and the initial concentration of the pollutant was established in 10 mg/L, as it was optimized in previous studies on diclofenac removal by CWPO.

Box–Behnken Design (BBD) is a response surface methodology (RSM) based on three-level incomplete factorial designs [54]. The coded levels used in BBD can be seen in Table 9. In this study, only 16 experiments were needed, including four replicates (See Table 3).

RMS methodology comprises a group of mathematical and statistical methods based on the fitting of empirical models to the experimental data acquired for the test design. Thus, RMS was applied to the experimental data using the commercial software Minitab [55]. In addition, multiple linear regression analysis of the experimental data followed by F-test lack of fit and other tests were performed in order to select the best model.

A manual regression method was used to fitting the quadratic polynomial Equation (16) to the experimental data [54]:

$$\gamma = \beta_0 + \sum_{i=1}^j \beta_i x_i + \sum_{i=2}^k \beta_{ii} x_i^2 + \sum_{i}^{i < j} \sum_j \beta_{ij} x_i x_j \quad (16)$$

where γ is the removal of NAP (%), β_0 is a fixed coefficient, β_i , β_{ii} , and β_{ij} are the coefficients for the linear, quadratic, and interaction effects, and X_i and X_j are the coded values of the independent input variables.

The effect of temperature (30, 50, and 70°C) on the CWPO reaction using a H_2O_2 dose of 1.5 mM, a pH value of 5, and 1 g/L of catalyst was studied, determining the reaction kinetics of the NAP degradation.

Table 9. Experimental design levels with three variables.

Levels Box–Behnken Design	A (H_2O_2) (mM)	B (Temperature) ($^\circ\text{C}$)	C (Initial pH)
Low (−1)	0.5	30	5
Medium (0)	1.5	50	7
High (+1)	2.5	70	9

3.5. Analytical Methods

NAP concentration was analyzed by High-Performance Liquid Chromatography, HPLC UV-Vis (Varian ProStar, Palo Alto, CA, USA), using a Perkin Elmer column (250×4.6 mm i.d., $5 \mu\text{m}$) as

stationary phase. The analyses were performed at 274 nm, using 50%/50% (*v/v*) of acetonitrile/acidified water solution (0.1% H₃PO₄) as mobile phase (0.5 mL/min) and a loop volume of 20 µL.

H₂O₂ concentration was measured at a wavelength of 410 nm using a UV-Vis spectrophotometer (Lambda 35 PerkinElmer, Waltham, MA, USA) after adding titanium (IV) oxysulfate solution to the sample. Finally, the real-water aqueous matrices were characterized by the measurement of the total organic carbon (TOC) and the total nitrogen (TN) concentrations with a TOC analyzer (Shimadzu TOC VSCH, Kyoto, Japan), and the chemical oxygen demand (COD), conductivity, suspended solids concentration, aromaticity, phenolic compounds, and nitrate (NO₃[−]) ions were measured according to the Standard Methods [56].

3.6. Toxicity Tests

The internationally standardized aquatic ecotoxicity test (Microtox M500 Analyzer, Carlsbad, CA, USA) was applied to measure the toxicity of the samples before and after the CWPO treatment. The test is based on the inhibition of the light emission by the marine bacterium *Vibrio Fischeri* to water samples (Luminescent bacteria test with Biotox testing kit; ISO 11348-3, 2009, Environmental Bio-Detection Products Inc, Campobello, Ontario, Canada). The test involves the standard procedure for Microtox analysis [57]. Adjusting the osmotic pressure close to 2% NaCl and pH between 6 and 8, the test was carried out at 15 °C. To the test solution, 5- and 15-min exposures were measured for bioluminescence inhibition assay. The percentage inhibition of the luminescence relative to a non-contaminated blank (ultrapure water) was used to express the toxicity of each sample. The EC₅₀ was calculated and subsequently converted into toxicity units (TUs), when the relative inhibition percentage was found to be above 20%. Moreover, the toxicity data from Microtox software[®] indicated that for the two contact times (5 and 15 min), there was no statistically significant difference ($p < 0.01$); so, the toxicity data at 5 min was considered in this study.

3.7. Identification of NAP Transformation Byproducts

An aliquot of 6 mL of the treated NAP effluent was analyzed by a dispersive liquid–liquid micro extraction procedure [58]. Then, the sample was injected for analysis in an ion trap mass spectrometer (HCTultra PTM Discovery System, Bruker, Billerica, MA, USA) coupled to HPLC with ESI, APCI, and NS interfaces (mass range: 50–6000 *uma*). The turbo ion spray source was operated in negative ion mode for all the analytes.

4. Conclusions

The effect of the operation parameters, e.g., temperature, H₂O₂ dosage, and pH, on the degradation of naproxen by catalytic wet peroxide oxidation (CWPO) using a laboratory-synthesized magnetic Fe₃O₄/MWCNTs catalyst was evaluated. The optimization of the experimental study was assessed using a response surface methodology (RSM)-Box–Behnken Design (BBD). The results showed that a high removal efficiency of the pollutant (82%) was obtained at 70 °C of temperature, 1.5 mM of H₂O₂ dose, and a pH value of 5. Furthermore, the performance of the catalyst was favored at low pH values and high temperatures. Indeed, it was found that hydrogen peroxide dosages higher than 1.5 mM decreased the removal of naproxen. The reaction kinetics were shown to be adequately described by the pseudo-second-order model, finding an activation energy value of 4.75 KJ/mol. Related to its stability, the catalyst showed a high removal efficiency (~80%) without loss of activity along three consecutive runs.

Two possible naproxen reaction mechanisms based on •OH radicals attack have been proposed. The degradation of several real-aqueous matrices—a wastewater treatment plant effluent (WWTP), surface water (SW), and a hospital wastewater (HW) spiked with naproxen—was evaluated, finding removal percentages of TOC of 50%, 15%, and 10% for NAP-SW, NAP-HW, and NAP-WWTP, respectively. Low efficiencies can be attributed to the high content of aromatic and nitrogenated compounds of the samples that act as scavengers of H₂O₂. Finally, the toxicity of the treated real

effluents was measured, obtaining successful results, with a maximum toxicity removal value of 96.5% for the hospital wastewater sample.

So, the obtained results support that the synthesized catalyst can be efficiently used in CWPO processes, revealing a promising and sustainable alternative for the treatment of wastewaters containing highly recalcitrant and toxic micro-pollutants.

Supplementary Materials: The following are available online at <http://www.mdpi.com/2073-4344/9/3/287/s1>, Figure S1: XRD patterns of a) magnetite (Fe_3O_4) and catalytic support; b) Fe_3O_4 /MWCNTs-1 and Fe_3O_4 /MWCNTs-2 catalysts; Figure S2: Evolution of H_2O_2 efficiency along the three CWPO runs; Figure S3: Quenching tests of hydroxyl radicals in the CWPO reaction; Figure S4: Chromatogram of NAP treated by CWPO reaction; Figure S5: Chromatogram of NAP standard; Figure S6: Evolution of the aromaticity content (a) for the three tested real-aqueous matrices spiked with NAP; (b) for SW sample and SW sample spiked with NAP; Table S1: Comparison of iron-based catalytic systems for the removal of NAP in liquid phase; Table S2: NAP degradation products detected by (-)-ESI-LC-MS analysis; Table S3: Representative analysis of the three real aqueous matrices.

Author Contributions: Conceptualization, J.G.; formal analysis, Y.H.-A., S.Á.-T.; investigation, Y.H.-A., S.Á.-T.; visualization, S.Á.-T., M.L., V.I.Á., J.A.D.; writing—original draft, Y.H.-A., S.Á.-T., J.G.; writing—review and editing, Y.H.-A., S.Á.-T., M.L., V.I.Á., J.A.D., G.O., J.G.

Funding: “This research was funded by Regional Government of Madrid provided through Remtavares Network, grant number P2018/EMT-4341” and “The APC was funded by Catalysts Journal”.

Acknowledgments: This research was funded by the Regional Government of Madrid provided through REMTAVARES Network P2018/EMT-4341 and the European Social Fund. Ysabel Huacalco thanks to the National Program of Scholarship (PRONABEC) in Peru.

Conflicts of Interest: The authors declare no conflict of interest.

References

1. Ebele, A.J.; Abou-Elwafa Abdallah, M.; Harrad, S. Pharmaceuticals and personal care products (PPCPs) in the freshwater aquatic environment. *Emerg. Contam.* **2017**, *3*, 1–16. [[CrossRef](#)]
2. Płuciennik-Koropczuk, E. Non-steroid anti-inflammatory drugs in municipal wastewater and surface waters. *Civ. Environ. Eng. Rep.* **2014**, *14*, 63–74. [[CrossRef](#)]
3. Larsson, D.G.J. Pollution from drug manufacturing: Review and perspectives. *Philos. Trans. R. Soc. B* **2014**, *369*. [[CrossRef](#)]
4. Benitez, F.J.; Acero, J.L.; Real, F.J.; Roldan, G.; Casas, F. Comparison of different chemical oxidation treatments for the removal of selected pharmaceuticals in water matrices. *Chem. Eng. J.* **2011**, *168*, 1149–1156. [[CrossRef](#)]
5. Shore, R.F.; Taggart, M.A.; Smits, J.; Mateo, R.; Richards, N.L.; Fryday, S. Detection and drivers of exposure and effects of pharmaceuticals in higher vertebrates. *Philos. Trans. R. Soc. B* **2014**, *369*. [[CrossRef](#)] [[PubMed](#)]
6. Boynton, C.S.; Dick, C.F.; Mayor, G.H. NSAIDs: An overview. *J. Clin. Pharmacol.* **1988**, *28*, 512–517. [[CrossRef](#)] [[PubMed](#)]
7. Balakrishna, K.; Rath, A.; Praveenkumarreddy, Y.; Guruge, K.S.; Subedi, B. A review of the occurrence of pharmaceuticals and personal care products in Indian water bodies. *Ecotoxicol. Environ. Saf.* **2017**, *137*, 113–120. [[CrossRef](#)] [[PubMed](#)]
8. Dong, W.; Xie, W.; Su, X.; Wen, C.; Cao, Z.; Wan, Y. Review: Micro-organic contaminants in groundwater in China. *Hydrogeol. J.* **2018**, *26*, 1351–1369. [[CrossRef](#)]
9. Ying, G.-G.; Kookana, R.S.; Kolpin, D.W. Occurrence and removal of pharmaceutically active compounds in sewage treatment plants with different technologies. *J. Environ. Monit.* **2009**, *11*, 1498–1505. [[CrossRef](#)] [[PubMed](#)]
10. Ashfaq, M.; Noor, N.; Saif-Ur-Rehman, M.; Sun, Q.; Mustafa, G.; Faizan Nazar, M.; Yu, C.-P. Determination of commonly used pharmaceuticals in hospital waste of Pakistan and evaluation of their ecological risk assessment. *CLEAN-Soil Air Water* **2017**, *45*, 1500392. [[CrossRef](#)]
11. Isidori, M.; Lavorgna, M.; Nardelli, A.; Parrella, A.; Previtera, L.; Rubino, M. Ecotoxicity of naproxen and its phototransformation products. *Sci. Total Environ.* **2005**, *348*, 93–101. [[CrossRef](#)] [[PubMed](#)]
12. El Mouelhi, M.; Ruelius, H.W.; Fenselau, C.; Dulik, D.M. Species-dependent enantioselective glucuronidation of three 2-arylpropionic acids. Naproxen, ibuprofen, and benoxaprofen. *Drug Metab. Dispos.* **1997**, *15*, 767–772.

13. Qurie, M.; Khamis, M.; Malek, F.; Nir, S.; Bufo, S.A.; Abbadi, J.; Scrano, L.; Karaman, R. Stability and removal of naproxen and its metabolite by advanced membrane wastewater treatment plant and micelle-clay complex. *CLEAN-Soil Air Water* **2013**, *42*, 594–600. [[CrossRef](#)]
14. Garcia-Costa, A.L.; Zazo, J.A.; Rodriguez, J.J.; Casas, J.A. Microwave-assisted catalytic wet peroxide oxidation. Comparison of Fe catalysts supported on activated carbon and γ -alumina. *Appl. Catal. B Environ.* **2017**, *218*, 637–642. [[CrossRef](#)]
15. Ma, D.; Liu, G.; Lü, W.; Yao, K.; Zhou, L.H.; Xie, C.P. Photodegradation of naproxen in aqueous systems by UV irradiation: Mechanism and toxicity of photolysis products. *Huan Jing Ke Xue* **2013**, *34*, 1782–1789. [[PubMed](#)]
16. Karaca, M.; Kıranşan, M.; Karaca, S.; Khataee, A.; Karimi, A. Sonocatalytic removal of naproxen by synthesized zinc oxide nanoparticles on montmorillonite. *Ultrason. Sonochem.* **2016**, *31*, 250–256. [[CrossRef](#)] [[PubMed](#)]
17. Oller, I.; Malato, S.; Sánchez Pérez, J.A. Combination of advanced oxidation processes and biological treatments for wastewater decontamination—A review. *Sci. Total Environ.* **2011**, *409*, 4141–4166. [[CrossRef](#)] [[PubMed](#)]
18. Kanakaraju, D.; Glass, B.D.; Oelgemöller, M. Advanced oxidation process-mediated removal of pharmaceuticals from water: A review. *J. Environ. Manag.* **2018**, *219*, 189–207. [[CrossRef](#)]
19. Roccaro, P.; Sgroi, M.; Vagliasindi, F.G.A. Removal of xenobiotic compounds from wastewater for environment protection: Treatment processes and costs. *Chem. Eng. Trans.* **2013**, *32*, 505–510.
20. Wang, H.; Jiang, H.; Wang, S.; Shi, W.; He, J.; Liu, H.; Huang, Y. Fe₃O₄-MWCNT magnetic nanocomposites as efficient peroxidase mimic catalysts in a Fenton-like reaction for water purification without pH limitation. *RSC Adv.* **2014**, *4*, 45809–45815. [[CrossRef](#)]
21. Tang, J.; Wang, J. Fe₃O₄-MWCNT magnetic nanocomposites as efficient Fenton-Like catalysts for degradation of sulfamethazine in aqueous solution. *ChemistrySelect* **2017**, *2*, 10727–10735. [[CrossRef](#)]
22. Hu, X.; Liu, B.; Deng, Y.; Chen, H.; Luo, S.; Sun, C.; Yang, P.; Yang, S. Adsorption and heterogeneous Fenton degradation of 17 α -methyltestosterone on nano Fe₃O₄/MWCNTs in aqueous solution. *Appl. Catal. B Environ.* **2011**, *107*, 274–283. [[CrossRef](#)]
23. Yu, L.; Yang, X.; Ye, Y.; Wang, D. Efficient removal of atrazine in water with a Fe₃O₄/MWCNTs nanocomposite as a heterogeneous Fenton-like catalyst. *RSC Adv.* **2015**, *5*, 46059–46066. [[CrossRef](#)]
24. Yao, Y.; Chen, H.; Lian, C.; Wei, F.; Zhang, D.; Wu, G.; Chen, B.; Wang, S. Fe, Co, Ni nanocrystals encapsulated in nitrogen-doped carbon nanotubes as Fenton-like catalysts for organic pollutant removal. *J. Hazard. Mater.* **2016**, *314*, 129–139. [[CrossRef](#)] [[PubMed](#)]
25. Das, R.; Abd Hamid, S.B.; Ali, M.E.; Ismail, A.F.; Anuar, M.S.M.; Ramakrishna, S. Multifunctional carbon nanotubes in water treatment: The present, past and future. *Desalination* **2014**, *354*, 160–179. [[CrossRef](#)]
26. Fan, X.-J.; Li, X. Preparation and magnetic property of multiwalled carbon nanotubes decorated by Fe₃O₄ nanoparticles. *New Carbon Mater.* **2012**, *27*, 111–116. [[CrossRef](#)]
27. Tomova, A.; Gentile, G.; Grozdanov, A.; Errico, M.E.; Paunović, P.; Avella, M.; Dimitrov, A.T. Functionalization and characterization of MWCNT produced by different methods. *Acta Phys. Pol. A* **2016**, *129*, 405–408. [[CrossRef](#)]
28. Singh, B.; Choudhary, V.; Teotia, S.; Gupta, T.; Singh, V.; Dhakate, S.; Mathur, R. Solvent free, efficient, industrially viable, fast dispersion process based amine modified MWCNT reinforced epoxy composites of superior mechanical properties. *Adv. Mater. Lett.* **2015**, *6*, 104–113. [[CrossRef](#)]
29. Álvarez-Torrellas, S.; Munoz, M.; Gläsel, J.; de Pedro, Z.M.; Domínguez, C.M.; García, J.; Etzold, B.J.M.; Casas, J.A. Highly efficient removal of pharmaceuticals from water by well-defined carbide-derived carbons. *Chem. Eng. J.* **2018**, *347*, 595–606. [[CrossRef](#)]
30. Alexander, D.L.J.; Tropsha, A.; Winkler, D.A. Beware of R²: Simple, unambiguous assessment of the prediction accuracy of QSAR and QSPR models. *J. Chem. Inf. Model.* **2015**, *55*, 1316–1322. [[CrossRef](#)]
31. Carley, K.M.; Kamneva, N.Y.; Reminga, J. *Response Surface Methodology*; Technical Report; Carnegie-Mellon University of Pittsburgh: Pittsburgh, PA, USA, 2004.
32. Piepho, H.P.; Edmondson, R.N. A tutorial on the statistical analysis of factorial experiments with qualitative and quantitative treatment factor levels. *J. Agron. Crop Sci.* **2018**, *204*, 429–455. [[CrossRef](#)]

33. Haji, S.; Khalaf, M.; Shukrallah, M.; Abdullah, J.; Ahmed, S. A kinetic comparative study of azo dye decolorization by catalytic wet peroxide oxidation using Fe-Y zeolite/H₂O₂ and photooxidation using UV/H₂O₂. *React. Kinet. Mech. Catal.* **2015**, *114*, 795–815. [[CrossRef](#)]
34. Zhang, C.; Zhou, M.; Ren, G.; Yu, X.; Ma, L.; Yang, J.; Yu, F. Heterogeneous electro-Fenton using modified iron-carbon as catalyst for 2,4-dichlorophenol degradation: Influence factors, mechanism and degradation pathway. *Water Res.* **2015**, *70*, 414–424. [[CrossRef](#)] [[PubMed](#)]
35. Wang, H.; Zhao, Y.; Sun, W.; Sun, C. The optimization, kinetics and mechanism of m-cresol degradation via catalytic wet peroxide oxidation with sludge-derived carbon catalyst. *J. Hazard. Mater.* **2017**, *326*, 36–46. [[CrossRef](#)]
36. Önal, Y.; Akmil-Başar, C.; Sarıci-Özdemir, Ç. Elucidation of the naproxen sodium adsorption onto activated carbon prepared from waste apricot: Kinetic, equilibrium and thermodynamic characterization. *J. Hazard. Mater.* **2007**, *148*, 727–734. [[CrossRef](#)] [[PubMed](#)]
37. Kremer, M.L. “Complex” versus “free radical” mechanism for the catalytic decomposition of H₂O₂ by ferric ions. *Int. J. Chem. Kinet.* **1985**, *17*, 1299–1314. [[CrossRef](#)]
38. Domínguez, C.M.; Quintanilla, A.; Casas, J.A.; Rodríguez, J.J. Kinetics of wet peroxide oxidation of phenol with a gold/activated carbon catalyst. *Chem. Eng. J.* **2014**, *253*, 486–492. [[CrossRef](#)]
39. Pastrana-Martínez, L.M.; Pereira, N.; Lima, R.; Faria, J.L.; Gomes, H.T.; Silva, A.M.T. Degradation of diphenhydramine by photo-Fenton using magnetically recoverable iron oxide nanoparticles as catalyst. *Chem. Eng. J.* **2015**, *261*, 45–52. [[CrossRef](#)]
40. Pignatello, J.J.; Oliveros, E.; MacKay, A. Advanced oxidation processes for organic contaminant destruction based on the fenton reaction and related chemistry. *Crit. Rev. Environ. Sci. Technol.* **2006**, *36*, 1–84. [[CrossRef](#)]
41. Wang, N.; Zhao, Q.; Zhang, A. Catalytic oxidation of organic pollutants in wastewater: Via a Fenton-like process under the catalysis of HNO₃-modified coal fly ash. *RSC Adv.* **2017**, *7*, 27619–27628. [[CrossRef](#)]
42. Cleveland, V.; Bingham, J.-P.; Kan, E. Heterogeneous Fenton degradation of bisphenol A by carbon nanotube-supported Fe₃O₄. *Sep. Purif. Technol.* **2014**, *133*, 388–395. [[CrossRef](#)]
43. Dulova, N.; Kattel, E.; Trapido, M. Degradation of naproxen by ferrous ion-activated hydrogen peroxide, persulfate and combined hydrogen peroxide/persulfate processes: The effect of citric acid addition. *Chem. Eng. J.* **2016**, *318*, 254–263. [[CrossRef](#)]
44. Kanakaraju, D.; Motti, C.A.; Glass, B.D.; Oelgemöller, M. TiO₂ photocatalysis of naproxen: Effect of the water matrix, anions and diclofenac on degradation rates. *Chemosphere* **2015**, *139*, 579–588. [[CrossRef](#)] [[PubMed](#)]
45. Ray, S.K.; Dhakal, D.; Lee, S.W. Rapid degradation of naproxen by AgBr-α-NiMoO₄ composite photocatalyst. *Chem. Eng. J.* **2018**, *347*, 836–848. [[CrossRef](#)]
46. Chen, S.; Cai, M.; Liu, Y.; Zhang, L.; Feng, L. Effects of water matrices on the degradation of naproxen by reactive radicals in the UV/Peracetic acid process. *Water Res.* **2018**, *150*, 153–161. [[CrossRef](#)]
47. Rueda Márquez, J.; Levchuk, I.; Sillanpää, M. Application of catalytic wet peroxide oxidation for industrial and urban wastewater treatment: A review. *Catalysts* **2018**, *8*, 673. [[CrossRef](#)]
48. Benitez, F.J.; Acero, J.L.; Gonzalez, T.; Garcia, J. Organic matter removal from wastewaters of the black olive industry by chemical and biological procedures. *Process Biochem.* **2001**, *37*, 257–265. [[CrossRef](#)]
49. Ortiz de García, S.A.; Pinto Pinto, G.; García-Encina, P.A.; Irusta-Mata, R. Ecotoxicity and environmental risk assessment of pharmaceuticals and personal care products in aquatic environments and wastewater treatment plants. *Ecotoxicology* **2014**, *23*, 1517–1533. [[CrossRef](#)]
50. Esteban García, B.; Rivas, G.; Arzate, S.; Sánchez Pérez, J.A. Wild bacteria inactivation in WWTP secondary effluents by solar photo-fenton at neutral pH in raceway pond reactors. *Catal. Today* **2018**, *313*, 72–78. [[CrossRef](#)]
51. Environmental Protection Agency. *NPDES Compliance Inspection Manual*; EPA 305-X-03-004; USEPA: Washington, DC, USA, 2004.
52. European Commission. *Commission Staff Working Document, Accompanying the Document Communication from the Commission to the European Parliament, the Council, the European Economic and Social Committee and the Committee of Regions*; Environmental Chemical Agency (ECHA), European Commission: Brussels, Belgium, 2013.
53. Singer, G.; Siedlaczek, P.; Sinn, G.; Rennhofer, H.; Mičušík, M.; Omastová, M.; Unterlass, M.; Wendrinsky, J.; Milotti, V.; Fedi, F.; et al. Acid free oxidation and simple dispersion method of MWCNT for high-performance CFRP. *Nanomaterials* **2018**, *8*, 912. [[CrossRef](#)]

54. Ferreira, S.L.C.; Bruns, R.E.; Ferreira, H.S.; Matos, G.D.; David, J.M.; Brandão, G.C.; da Silva, E.G.P.; Portugal, L.A.; dos Reis, P.S.; Souza, A.S.; et al. Box-Behnken design: An alternative for the optimization of analytical methods. *Anal. Chim. Acta* **2007**, *597*, 179–186. [[CrossRef](#)] [[PubMed](#)]
55. Ayazi, Z.; Khoshhesab, Z.M.; Norouzi, S. Modeling and optimizing of adsorption removal of Reactive Blue 19 on the magnetite/graphene oxide nanocomposite via response surface methodology. *Desalin. Water Treat.* **2016**, *57*, 25301–25316. [[CrossRef](#)]
56. Eaton, A.D. *Standard Methods for the Examination of Water and Wastewater*, 21st ed.; American Public Health Association/American Water Works Association/Water Environment Federation: Washington, DC, USA, 2005.
57. Gaudet, I.D. *Standard Procedure for MICROTOX Analysis*; Alberta Environmental Centre: Vergeville, AB, Canada, 1994.
58. Zgoła-Grześkowiak, A. Application of DLLME to Isolation and Concentration of Non-Steroidal Anti-Inflammatory Drugs in Environmental Water Samples. *Chromatographia* **2010**, *72*, 671–678. [[CrossRef](#)]



© 2019 by the authors. Licensee MDPI, Basel, Switzerland. This article is an open access article distributed under the terms and conditions of the Creative Commons Attribution (CC BY) license (<http://creativecommons.org/licenses/by/4.0/>).